

Inter-polarization Mapping via Gaussian Process Regression for Sentinel-1 EW Denoising

Adrian Focsa^{1,2}, Andrei Anghel¹, Mihai Datcu^{1,3}

¹ CEOSpaceTech, University POLITEHNICA of Bucharest (UPB), Bucharest, Romania

² Military Technical Academy "Ferdinand I" (ATMFI), Bucharest, Romania

³ Remote Sensing Technology Institute (IMF), German Aerospace Center (DLR), Wessling, Germany

Contact author e-mail: focsa.adrian@yahoo.com

Abstract—The Sentinel-1 SAR images acquired using the TOPSAR modes i.e., IW and EW on cross-polarization are significantly affected by the thermal noise on low-back-scattering areas. For example, in the arctic and some desert zones both inter-swath and inter-burst noise amplification occurs. In this paper we propose a workflow for removing the thermal noise from Sentinel-1 ground detected SAR images on low back-scattering conditions by employing the co-polarization SAR image and the Gaussian Process Regression. Our processing flow uses the noise vectors provided in the European Space Agency (ESA) ground detected product and scales them such that a slightly over-denoised image is produced. Then, the Gaussian Process Regression is used to map the co-polarization SAR image into the cross-polarization SAR image. Prior to this step, a radiometric correction is applied on the co-polarization data, since its pixel values are heavily dependent on the incidence angle. Finally, the denoised cross-polarization image is obtained as a linear combination between the over-denoised version and the predicted image. Since, the co-polarization channel is employed for the prediction of the missing values in the cross-polarization channel there is no need for co-registration and the denoising procedure is trustworthy.

Index Terms—TOPSAR denoising, Gaussian Process Regression, cross-polarization

I. INTRODUCTION

ESA Copernicus program comprises Sentinel-1 A/B, a pair of polar orbit satellites equipped with C-band SAR sensors able to map the Earth using 4 scanning modes in either single or dual polarization: STRIPMAP, Interferometric Wide(IW), ExtraWide (EW) and Wave Mode (WV). Among all products, under weak back-scattering conditions (e.g., calm waterbodies, desert) the cross-polarization detected (Ground Range Detected Magnitude (GRDM) products) TOPSAR images i.e., IW and EW are more affected by scalloping in the azimuth direction and by the thermal noise in the range direction. Even though starting with Instrument Processing Facility (IPF) 2.90 both azimuth and range noise vectors are provided in the product ancillary files, the denoising method [1] based on (1) may produce poor quality denoised images.

$$I_{d[ESA]} = \max(0, I_n - N_{ESA}) \quad (1)$$

In (1), $I_{d[ESA]}$ suggests the denoised image obtained using ESA algorithm [1] from the noisy (raw) GRDM intensity image (I_n) and the noise vectors N_{ESA} .

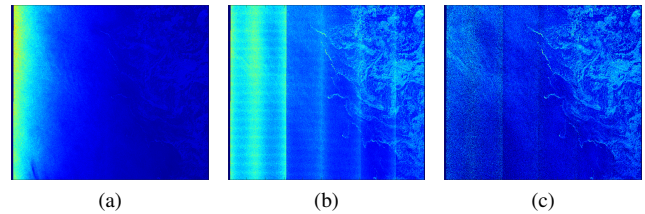


Fig. 1: Sentinel-1 GRDM product example S1A_EW_GRDM_1SDH_20210621T072157_20210621T072257_038435_04890F_A9C0 displayed in linear pixel units: a) Co-polarization, b) Cross-polarization, c) Cross-polarization SAR image denoised using [1]

The general idea behind the existing approaches that improve [1] is depicted by (2) and consists in modifying the available noise vectors (N_{ESA}) to be more consistent with the measured noise floor. Thus, N_{ESA} may be transformed ($\mathcal{T}(\cdot)$) (shifted [2] or modeled on intervals with exponential functions [3]) then scaled via K_{ns} . Furthermore, to preserve the inter-swath boundaries continuity some offset coefficients K_{pb} (power balancing) may be also employed.

$$I_{d[method]} = I_n - (K_{ns}\mathcal{T}(N_{ESA}) + K_{pb}) \quad (2)$$

Lee *et. al* [4] proposed a simplified approach compared to [5] in two aspects: no offset parameter is needed for correction and the scaling coefficient (K_{ns}) is derived in closed form solution (least squares estimation) using a single image instead of using a collection of SAR images. The denoising performance in [4] was evaluated through simulated data. In [6] the thermal noise is considered to have an additive and a multiplicative component. The removal of the latter is the key for the enhancement of the textural characterization of the SAR image.

In [2], the misfit between the noise vector provided by ESA and the ones measured from data is modeled by a spatial shift estimated maximizing the correlation (Pearson correlation coefficient) to a vector called "antenna range gain" accounting for the antenna pattern and the range influence. In [7] the TOPSAR denoising is performed in the wavelet domain through a soft-thresholding processing. The profile correction

step in [7] has similar effect as the power balancing coefficient in [2], [5], [8] and it is computed from the image profile (range projection). Inherently, the output from [7] has less details since wavelet sub-bands are soft-thresholded.

Many approaches for the evaluation of the cross-polarization noise reduction performance were assessed. In [8], the inter-swath boundaries continuity together with a key-points matching approach was investigated whereas in [5] an automatic K-means clustering on Haralick texture features was performed. Mascolo et. al [9] quantified the denoising performance through Monte Carlo simulations.

As shown in Fig. 1c the denoising algorithm [1] reduces the thermal noise from Fig. 1b. However, the average range profiles displayed in Fig. 2 reveal that the 2D noise field provided by ESA is locally inconsistent. Therefore, the denoised product is either over-denoised or under-denoised. These effects mostly occur in the inter-swath regions.

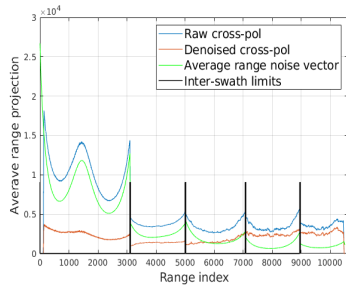


Fig. 2: Average range projection over raw and ESA denoised cross-polarization intensity image. Evidently, there are portions in the range profile of the denoised image still positively correlated to the range noise vectors

In this paper we propose a workflow for removing the thermal noise from Sentinel-1 GRDM SAR images on low back-scattering conditions by employing the co-polarization SAR image and the Gaussian Process Regression (GPR) [10]. Our method's reliability is ensured by the fact that the reconstruction of the pixels in the cross-polarization image is performed with data recorded by the same sensor and no additional co-registration processing is needed. The proposed denoising procedure uses the noise vectors provided in the product ancillary files and scales them such that a slightly over-denoised image is produced using (1). Then the Gaussian Process Regression [10] is used to map the co-polarization SAR image into the cross-polarization SAR image. However, prior to this step, the co-polarization data is applied a radiometric correction, since its pixel values are heavily dependent on the incidence angle. Finally, the denoised cross-polarization image is obtained as a linear combination between the over-denoised version and the GPR predicted image. The weights map is obtained through filtering with a circular kernel the binary map containing 1's at the positions where ESA denoising method (1), before applying *max* operator, resulted in a null or negative pixels values.

The rest of the paper is structured as follows. Section II presents the proposed processing flow and introduces the GPR

key-points in sub-section II-A and the radiometric correction in sub-section II-B. The proposed denoising procedure is detailed in sub-section II. In Section III, the denoising results are displayed and discussed whereas the conclusions are drawn in Section IV.

II. PROPOSED WORKFLOW

The proposed denoising processing flow is based on the recovery of the data lost after applying (1) with data inferred through GPR. As shown in Fig. 3, first, both co-polarized and cross-polarized GRDM SAR images are corrected using [1]. Then, the incidence angle compensation is applied. This step is depicted in sub-section II-B. Further, using reliable areas (high

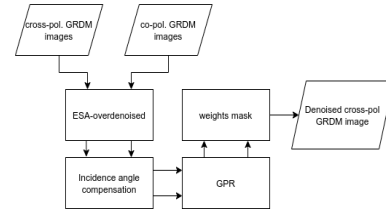


Fig. 3: Proposed denoising workflow

SNNR defined in [5]) in each the dual-pol SAR images the kernel-based GPR model is trained. The training process learns the physical signature translation from co-polarized data to cross-polarized data. The input data is represented by the ESA denoised - incidence angle corrected cross-polarized pixels whereas the output is the corresponding co-polarized pixels.

$$I_{d[proposed]} = I_m \times I_{d[ESA']} + (1 - I_m) \times I_{[GPR]} \quad (3)$$

In (3), the final denoised image is obtained by combining the GPR prediction $I_{[GPR]}$ with the output obtained using (2) with $K_{pb} = 0$, \mathcal{T} -identity transformation and K_{ns} chosen such that an over-denoised version ($I_{d[ESA']}$) of the raw image is obtained. The two components are weighted using the mask I_m . The mask is obtained in a two step process. When the subtraction of the 2D noise field from the noisy image is performed, the negative and null values positions are stored and a new image containing ones on those positions and zeros otherwise is formed. Then, this binary mask is 'smeared' using a 7×7 circular filtering kernel resulting the final weights mask.

A. Gaussian Process Regression

Even though Gaussian Process Regression is a powerful Bayesian prediction tool, it has been presented relatively recently [10] as a Machine Learning technique. GPR was previously known as Kriging interpolation. It has been successfully employed for physical parameters mapping in the context of polarimetric SAR data [11].

$$\mathbf{y} = \mathbf{f}(\mathbf{X}) + \varepsilon, \varepsilon \sim \mathcal{N}(0, \sigma \mathbf{I}_n) \quad (4)$$

The nonlinear regression model for a given training set $\mathcal{D}(\mathbf{y}, \mathbf{X})$ is depicted by (4). Given the observed input data set $\mathbf{X} = \{\mathbf{x}_1, \mathbf{x}_2, \dots, \mathbf{x}_N\}$ and the corresponding output set

$\mathbf{y} = \{y_1, y_2, \dots, y_N\}$ with $\mathbf{x}_i \in \mathbb{R}^D$ and $y_i \in \mathbb{R}$, a multivariate Gaussian distribution models the function values. In Section III, the presented results are obtained using an one-to-one mapping ($D = 1$).

$$p(\mathbf{y}^{test} | \mathbf{X}^{test}, \mathcal{D}) = \mathcal{N}(\mathbf{y}^{test} | \boldsymbol{\mu}_*, \boldsymbol{\sigma}_*^2) \quad (5)$$

The predicted values and their corresponding variances are analytically derived from the posterior distribution (5) associated with the test outputs \mathbf{y}^{test} .

$$\boldsymbol{\mu}_* = \mathbf{K}_{f*}^T (\mathbf{K}_{ff} + \sigma^2 \mathbf{I}_N)^{-1} \mathbf{y} \quad (6)$$

In (6) and (7), \mathbf{K}_{f*} is the covariance matrix between the training and the test points, \mathbf{K}_{ff} is the train samples covariance matrix whereas \mathbf{K}_{**} represents the test samples covariance matrix.

$$\boldsymbol{\sigma}_*^2 = \sigma^2 + \mathbf{K}_{**} - \mathbf{K}_{f*}^T (\mathbf{K}_{ff} + \sigma^2 \mathbf{I}_N)^{-1} \mathbf{K}_{f*} \quad (7)$$

In the experiments presented in Section III we have used the squared exponential kernel defined in (8).

$$k(\mathbf{x}_i, \mathbf{x}_j) = \sigma_k^2 \exp\left(-\frac{1}{2} \sum_{l=1}^N \frac{(x_{il} - x_{jl})^2}{\lambda_k}\right) \quad (8)$$

In (8), the hyper-parameters σ_k and λ_k model the bell-like shape of the kernel and implicitly the smoothness of the predictor f .

B. Incidence angle compensation

As is the case of TOPSAR mode, for wide incidence angle range acquisitions, many SAR image applications need a correction pre-processing step. In our case, the incidence angle compensation purpose is to reduce the incidence angle dependence of the back-scattering energy not only for the co-polarization SAR image, for which this effect is obvious [see Fig. 1a] but also for the cross-polarization image prior to feeding them to GPR.

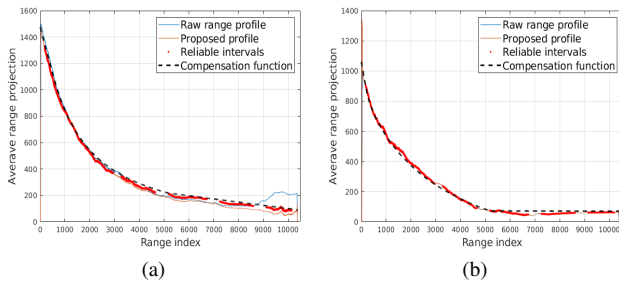


Fig. 4: Incidence angle compensation profile estimation: a) example-1 and b) example-2

The most common techniques for incidence angle compensation are linear and n-th power cosine correction. However, as noted in [12], these approaches may not comply with all scanning scenarios and illuminated scenes. Therefore, we

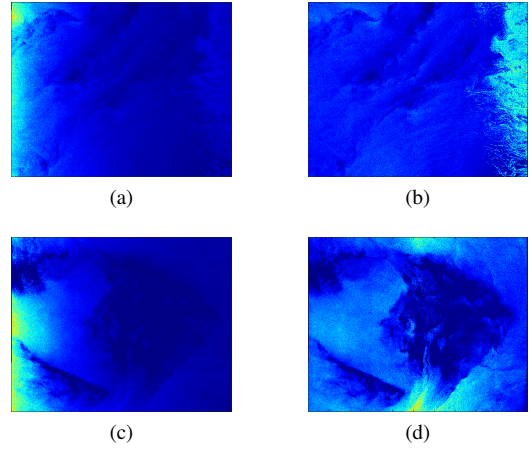


Fig. 5: Incidence angle compensation examples: a) Raw co-polarization GRDM image example-1, b) Corrected version of b), c) Raw co-polarization GRDM image example-2, d) Corrected version of c)

propose a new compensation algorithm efficient for the dual-pol data used in this study. The processing steps need to perform the incidence angle compensation are listed below:

1. Compute the image profile (range) only for pixels obeying $SNNR_{cross-pol} < 3dB$;
2. Select reliable regions from profile (mid swath intervals for the sub-swaths 2-5 and the highest SNNR regions from the first sub-swath)
3. Fit a polynomial ratio function for the first two sub-swaths (the exponential decay function fits less) and a first order polynomial for the last 3 sub-swaths. The discontinuity between the two regression parts is treated by adding/subtracting half of the offset corresponding to the intersection abscissa point.
4. Linearly fit the obtained regression curve to the raw range profile.

The first step avoids the dependence of the range profile of strong back-scattering targets. The second step is useful such that the sub-swath boundary regions to be discarded since they are more likely to be affected by over/under-denoising.

The range profiles used to compensate the incidence angle dependence are highlighted in Fig. 4 whereas the raw and the corrected versions of the cross-polarization images is shown in Fig. 5.

III. RESULTS

In this section the denoised images resulted by applying the proposed denoising workflow are displayed and compared to the ones obtained by [1]. The four denoised example images correspond to the products (example-1,...,example-4) listed below:

- S1A_EW_GRDM_1SDH_20210621T072157_20210621T072257_038435_04890F_A9C0
- S1A_EW_GRDM_1SDH_20210620T064151_20210620T064251_038420_0488A2_65A8
- S1B_EW_GRDM_1SDH_20190124T074426_20190124T074526_014633_01B458_E8F5
- S1A_EW_GRDM_1SDH_20210307T070530_20210307T070630_036889_0456BB_881C

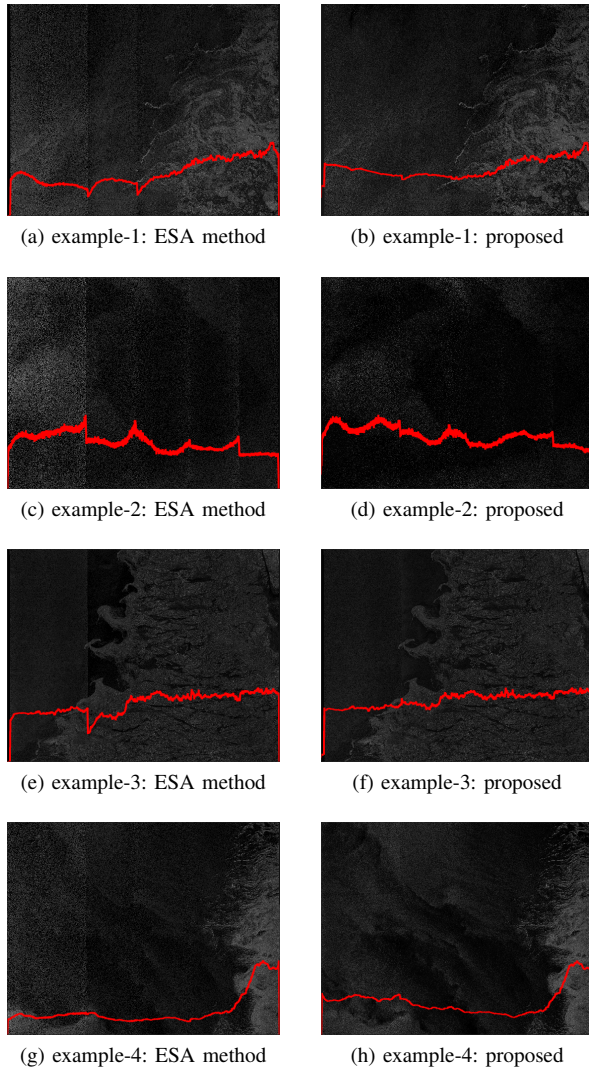
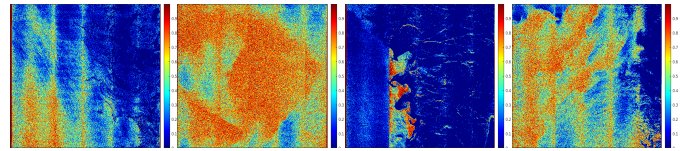


Fig. 6: Comparative results obtained with the method described in [1] called ESA method and the proposed one. The mean range profiles overlay the results.

The weights masks resulted for the displayed examples in Fig. 7 are shown in Fig. 6. We have used $K_{ns} = 1.2$ as scaling factor to produce the over-denoised images in the presented examples. Visual proof that the proposed method overcomes the limitations of the one depicted in [1] is provided in Fig. 7. Moreover, Fig. 6f presents a result over a product also analyzed in [7]. As opposed to [7], our method manages to preserve more details in the open water region.

IV. CONCLUSIONS

In this paper we proposed a technique for reducing the thermal noise in Sentinel-1 EW GRDM products recorded over weak back-scattering scenarios. To our knowledge, it is the first denoising procedure to benefit from the co-polarization image. Beside the visual enhancement of the denoised image, the average range profiles (red curves in Fig. 6) proves that



(a) I_m : example-1 (b) I_m : example-2 (c) I_m : example-3 (d) I_m : example-4

Fig. 7: The masks employed in the proposed denoising process for the four examples in Fig. 6. As expected, the pixels located in the inter-swath/inter-burst regions are more likely to be replaced by the kernel-based GPR prediction

our method also boosts the inter-swath energy balancing by exploiting the co-polarization channel. The employed weights mask (I_m) contribute to reducing the multiplicative component of the noise depicted in [6]. Because our denoising workflow harnesses the co-polarization product to enhance the cross-polarization channel it may be only for dual-pol acquisitions.

ACKNOWLEDGMENT

This work was supported by the Romanian Ministry of Education and Research, CNCS-UEFISCDI, project number PN-III-P4-ID-PCE-2020-2120, within PNCIDI III

REFERENCES

- [1] R. Piantanida, N. Miranda, and G. Hadjduch, "Thermal Denoising of Products Generated by the S-1 IPF," *Sentinel-1 Mission Perform. Centre, Ramonville-Saint-Agne, France, Tech. Rep. MPC-0392*, 2017.
- [2] A. Korosov, D. Demchev, N. Miranda, N. Franceschi, and J.-W. Park, "Thermal Denoising of Cross-Polarized Sentinel-1 Data in Interferometric and Extra Wide Swath Modes," *IEEE Transactions on Geoscience and Remote Sensing*, 2021. (Early Access).
- [3] P. Q. Lee, L. Xu, and D. A. Clausi, "Estimating Noise Floor in Sentinel-1 Images With Linear Programming and Least Squares," *IEEE Transactions on Geoscience and Remote Sensing*, pp. 1–14, 2021.
- [4] P. Q. Lee, "Correction methods for non-stationary noise floor in sentinel-1 images using convex optimization," Master's thesis, University of Waterloo, 2020.
- [5] J.-W. Park, J.-S. Won, A. A. Korosov, M. Babiker, and N. Miranda, "Textural noise correction for Sentinel-1 TOPSAR cross-polarization channel images," *IEEE Transactions on Geoscience and Remote Sensing*, vol. 57, no. 6, pp. 4040–4049, 2019.
- [6] Y. Sun and X.-M. Li, "Denoising Sentinel-1 Extra-Wide Mode Cross-Polarization Images Over Sea Ice," *IEEE Trans. Geosci. Remote Sens.*, vol. 59, no. 3, pp. 2116–2131, 2021.
- [7] S. Chlailly, T. Kramer, T. Eltoft, and A. Marinoni, "A wavelet-based thermal noise removal approach for Sentinel-1 records on polar areas," in *EUSAR 2021; 13th European Conference on Synthetic Aperture Radar*, pp. 1–5, 2021.
- [8] J.-W. Park, A. A. Korosov, M. Babiker, S. Sandven, and J.-S. Won, "Efficient thermal noise removal for Sentinel-1 TOPSAR cross-polarization channel," *IEEE Transactions on Geoscience and Remote Sensing*, vol. 56, no. 3, pp. 1555–1565, 2017.
- [9] L. Mascolo, J. M. Lopez-Sanchez, and S. R. Cloude, "Thermal Noise Removal From Polarimetric Sentinel-1 Data," *IEEE Geoscience and Remote Sensing Letters*, vol. 19, pp. 1–5, 2022.
- [10] C. E. Rasmussen, "Gaussian processes in machine learning," in *Summer school on machine learning*, pp. 63–71, Springer, 2003.
- [11] K. Blix, M. M. Espeseth, and T. Eltoft, "Machine Learning for Arctic Sea Ice Physical Properties Estimation Using Dual-Polarimetric SAR Data," *IEEE Transactions on Geoscience and Remote Sensing*, vol. 59, no. 6, pp. 4618–4634, 2020.
- [12] I. E. Mladenova, T. J. Jackson, R. Bindlish, and S. Hensley, "Incidence angle normalization of radar backscatter data," *IEEE Transactions on Geoscience and Remote Sensing*, vol. 51, no. 3, pp. 1791–1804, 2012.